



Original article

Exploring the anticancer potential of pyrazolo[1,2-*a*]benzo[1,2,3,4]tetrazin-3-one derivatives: The effect on apoptosis induction, cell cycle and proliferation



Francesco Mingoia^{a,*}, Caterina Di Sano^b, Francesco Di Blasi^b, Marco Fazzari^{c,1},
Annamaria Martorana^c, Anna Maria Almerico^c, Antonino Lauria^c

^a Istituto per lo Studio dei Materiali Nanostrutturati (ISMN) – CNR, Via Ugo La Malfa 153, 90146 Palermo, Italy

^b Istituto di Biomedicina ed Immunologia Molecolare (IBIM) – CNR, Via U. La Malfa 153, 90146 Palermo, Italy

^c Dipartimento di Scienze e Tecnologie Biologiche Chimiche e Farmaceutiche (STEBICEF), Sezione di Chimica Farmaceutica e Biologica – Università di Palermo, Via Archirafi 32, I-90123 Palermo, Italy

ARTICLE INFO

Article history:

Received 2 October 2012

Received in revised form

21 March 2013

Accepted 24 March 2013

Available online 6 April 2013

Keywords:

Pyrazolo[1,2-*a*]benzo[1,2,3,4]tetrazinone

VLAK protocol

Anticancer agents

Apoptosis inducers

Cell cycle

ABSTRACT

In order to investigate their anticancer potential, four new pyrazolo[1,2-*a*]benzo[1,2,3,4]tetrazinone derivatives, designed through the chemometric protocol VLAK, and three of the most active compounds of the previous series have been evaluated on some cellular events including proliferation, apoptosis induction, and cell cycle. The NCI one dose (10 μ M) screening revealed that the 8,9-di-methyl derivative showed activity against Leukemia (CCRF-CEM) and Colon cancer cell line (COLO 205), reaching 81% and 45% of growth inhibition (GI), respectively. Replacement of the two methyl groups with two chlorine atoms maintained the activity toward Leukemia cell (CCRF-CEM, GI 77%) and selectively enhanced the activity against COLO 205 attaining a LD₅₀ in the μ M range and against SW-620 a GI of 77%. Interestingly, an appreciable growth inhibition of 47% against therapeutically “refractory” Non-Small Cell Lung Cancer (NCI-H522) was observed. Moreover, the apoptosis induction, based on mitochondrial membrane depolarization, was found in the range EC₅₀ 3–5 μ M on HeLa cell, evidencing a well defined relationship with the related *in vitro* cell growth inhibitory assays (MTT) performed against other selected tumor cell lines not included in the NCI tumor panel (HeLa, cervix; H292, lung; LAN-5, CNS; CaCo-2, colon; 16HBE, normal human cell lung) and against MCF-7 tumor cell line (breast). Only for the most active compounds, further cell cycle tests on HeLa displayed a cell arrest on S phase. Thus, a promising new class of anticancer candidates, acting as valuable apoptotic inducers, is proposed.

© 2013 Elsevier Masson SAS. All rights reserved.

1. Introduction

Current advances in cancer research consider the apoptosis, other than occurring in various physiological events, as crucially involved in the regulation of tumor growth as well as in the treatment response. Most of the anticancer strategies used in clinical oncology such as chemotherapy, γ -irradiation, including suicide gene therapy or immunotherapy, have been related to the activation of apoptosis signal transduction pathways in cancer cells. The loss of such a cell event increases the cancer aggressiveness [1].

The understanding of selective induction of the apoptosis will provide a promising basis for novel opportunities in the fight

against cancer and drug resistance. Thus, deeper investigations on molecular basis of apoptosis modulation open promising ways for a more rational approach to develop new therapeutic strategies [2]. For these reasons, growing interest is currently focused on the attempt to improve cancer therapy by mean of the modulation of apoptosis processes.

Equally of interest, because strictly connected, is the exploration of the effect on the cell cycle of active molecules. Multiple genetic changes occur during the evolution of normal cells into cancer ones. Cell cycle inhibitors or modulators, able to control tumor growth, continue to be regarded as highly promising new therapeutic agents against human cancer [3]. As known, the loss of fidelity in the processes that replicate and repair the genome are typical molecular mechanisms of cellular transformation and may help to identify potential targets for cancer therapies [4]. Over the last years, efforts have been made to identify the targets of cell cycle phase that regulate several processes, but the whole view is not yet

* Corresponding author. Tel.: +39 0916809368; fax: +39 0916809399.

E-mail address: mingoia@pa.ismn.cnr.it (F. Mingoia).

¹ Current address: Fondazione Ri.MED, Via Bandiera 11, 90133 Palermo, Italy.

complete on understanding the processes involved in proliferation, differentiation, transformation, and programmed cell death [5].

Taking into account the strictly interconnection between cell death, cell survival, and cell progression pathways, the understanding of the interaction of new active compounds with key components of these cell events may be helpful on advancement for new therapeutic perspectives. Several components common to apoptosis and cell cycle have been identified and constitute basic elements to correlate different molecular linkages between cell death, survival and cycle [6,7]. Therefore, the design of new compounds able to modulate the apoptotic process, both as activators or inhibitors, represents an important strategic therapeutic approach in cancer disease.

In this context, our attention has been focused on a poor biologically investigated nitrogen tricycle ring system, the pyrazolo [1,2-a]benzo[1,2,3,4]tetrazinone core (PBT).

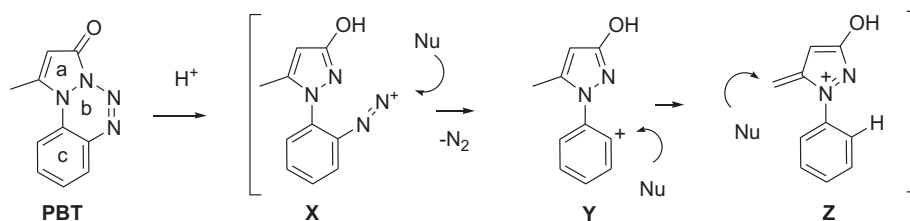
Our interest on PBT system has begun with the peculiar chemical behavior observed previously in the course of reactivity studies [8]. Under a suitable nucleophilic microenvironment, a ring opening can occur generating reactive entity such as **X**, **Y**, and **Z** species, as shown in Scheme 1.

Moreover, by analogy with azolotetrazinones, such as mitozolomide and temozolomide, effective antineoplastic agents currently used against malignant melanoma, mycosis fungoides and brain tumors [9–11], the PBT skeleton possesses isosteric structural features that could induce similar behavior.

In particular, under soft acid conditions, the first ring opening can occur on the b ring, generating the intermediate electrophilic diazonium species **X**. Depending on the chemical environment, if loss of molecular nitrogen takes place, the aromatic carbocation species **Y** could be formed and in turn could be attacked by nucleophiles. Alternatively, internal rearrangement by hydrogen transposition can afford other methylene reactive species such as intermediate **Z**. All these reactive intermediates have been trapped with charged nucleophile (Nu^-) or neutral nucleophile (NuH) affording the related adducts [8].

Additionally, due to the high metabolism rate, tumor cells evolved the ability to work in a more acid environment by approximately 0.3–0.5 pH unit than normal cell [12,13]. Thus, compounds possessing a peculiar chemical behavior in acid media could display increased reactivity becoming selective toward cancer cell. This premise has been an additional concept, which stimulated the interest toward the PBT derivatives for potential use as cancer selective therapeutic strategy. The starting idea was to verify “in cell” the peculiar chemical reactivity of PBT system (Scheme 1) that in presence of different nucleophilic species (electron rich, neutral or negatively charged molecules) such as proteins or $-\text{SH}$, $-\text{NH}_2$, $-\text{COO}^-$, $-\text{OH}$ containing biomolecules, can originate adducts.

Previous structure–activity relationships (SAR) pointed out that the presence of a chlorine atom is well tolerated in both position 8 and 9 of the PBT ring, without remarkable difference [14]. Whereas in the case of the methyl group, switching from the 8 to 9 position gives rise to the most active compound, either for the number of cell lines inhibited and for selectivity against a specific subpanel.



Scheme 1. Ring opening under soft acid conditions.

Therefore, to take a deeper insight, we extended the studies with the design and synthesis of new PBT derivatives by introducing on the phenyl moiety (ring c) some substituent ($\text{R}_1\text{--}\text{R}_4$) (Fig. 1), exploiting the use of a valuable library of available commercial nitro-anilines which are key reactants in our synthetic approach.

The design started from an *in silico* analysis that took advantage from the chemometric protocol VLAK (Virtual Lock-and-Key), recently developed by us [15]. In the last decades, the *in silico* methodologies have seen a good improvement from the point of view of robustness and prediction capability. The molecular modeling and the chemometric approach represented two *in silico* tools that address the issue of the lead optimization from two different points of view, ligand based drug design and structure based drug design, respectively. Both methodologies led to good results in our studies. For example the molecular docking was applied in the DNA ligands design of indolopyrimidine derivatives endowed with good antitumor activity [16]; the induced fit was applied in the analysis of the Hsp90 and IKK binding sites [17,18]. On the other hand, the chemometric approach and the multivariate analysis were applied on the ACAM database, in the search of the structural features that are determinant to increase the anti-proliferative activity [19], or in the tuning the biological activity for Hsp90 inhibitors [20].

2. Results and discussions

2.1. *In silico* analysis

The design of the new PBT derivatives, proposed herein, started from the *in silico* tool VLAK. In recent applications [21], this protocol was able to improve the anti-proliferative activity of annelated pyrimidine derivatives [22,23]. Thus, with the aim to analyze the PBT compounds already possessing good anti-proliferative activity and to design new ones, a database of PBTs with different substituents in the C ring (Fig. 1, $\text{R}_1\text{--}\text{R}_4$), including the PBTs previously synthesized and tested [14], was submitted to VLAK protocol.

The PBT database (an in house library of new compounds to be processed) was built by considering the reaction pathway leading to the PBT nucleus, which involves, as mentioned before, the use of substituted *ortho*-nitro aniline commercially available (see Experimental section).

The first step of the VLAK protocol is the conversion of the biological target in a “lock model” in which the keys (the structures) could be “fitted” [15].

The NCI AntiCancer Agent Mechanism (ACAM) Database was chosen as source of biological data for the construction of the VLAK “lock models”. It consists of a repository of structures with anticancer activity and a reasonably well-known mechanism of action. Drug screening data are available for each structure as measurement of their growth inhibition ability over a panel of about 60 human tumor cell lines, and all tested molecules are explicitly designed as a training set for neural network and multivariate analysis [24,25].

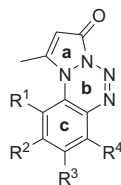


Fig. 1. Pyrazolo[1,2-a]benzo[1,2,3,4]tetrazinone derivatives (PBTs).

In particular, this database is constituted by 121 antitumor drugs classified for their mechanism of action (Supplementary material), which can be considered like the biological target in the protocol. The NCI ACAM Database was chosen because it was demonstrated as the molecular descriptors, by means of multivariate analysis, are able to discriminate the mechanisms of action of the drugs [19].

The VLAK protocol assigns to PBT database compounds the percentage of affinity (A%) with respect to six mechanisms of action, which include alkylating agents, antimetabolic agents, topoisomerase I inhibitors, topoisomerase II inhibitors, RNA/DNA antimetabolites, and DNA antimetabolites. Table 1 lists the results obtained for the PBTs previously reported (6e–6l) along with the new designed ones (6a–6d) with the higher percentage of affinity (A). The calculation procedure is detailed in the experimental section whereas the output results for the selected PBTs, related the six lock models representing each class of drugs (MAs), are reported in Supplementary material.

By analyzing the results, it is possible to evidence as the PBTs of type 6e–6l are well classified as Alkylating Agents (A) with the exception of the derivative 6j. Among the new designed PBTs, the top scored was the derivative 6b, classified as antimetabolic agent. The derivatives 6a, 6c were classified as topoisomerase II inhibitors and 6d as alkylating agent.

2.2. Chemistry

Thus, the new hit PBT compounds and three of the old series were synthesized as reported in Scheme 2. Starting from commercially available *ortho*-nitro-anilines 1a–1g, the azofuranones 3a–3g were prepared in 65–85% yields, adapting the procedures known in the literature [14] to the new reactants. Further rearrangement at room temperature, under acid conditions, afforded in 75–85% yields the corresponding nitrophenylpyrazol-3-one derivatives 4a–4g. Catalytic reduction over Pd on charcoal or chemical reduction with AcOH and Iron powder, followed by diazotization in concentrated sulfuric acid allowed the isolation of the PBT derivatives as colored red solid (yields 55–75%) after treatment with bicarbonate solution.

2.3. Biological assays

In order to investigate their anticancer potential and to verify the influence of molecular modifications on biological activity, as selected by the VLAK protocol, derivatives 6a–6g were evaluated for their *in vitro* antiproliferative and pro-apoptotic activity. Moreover, in the attempt to correlate possible molecular relationships between these cell events [6,7], three of the most active compounds (6a–6b, 6d) were evaluated on cell cycle tests.

2.3.1. *In vitro* antiproliferative activity (MTT)

A preliminary bioassay was carried out by using MTT protocol [26]. We selected several tumor cell lines, five of which not included in the NCI panel (HeLa, cervix; H292, lung; LAN-5, CNS; Caco-2, colon; 16HBE, lung healthy human cell), and for

Table 1
VLAK results on PBT derivatives.

Compound	MA (A%)						R
	A	B	C	D	E	F	
6a	52	62	75	86	76	40	R ¹ = R ⁴ = H; R ² = R ³ = Me
6b	46	90	57	79	56	33	R ¹ = R ⁴ = H; R ² = R ³ = Cl
6c	55	77	73	84	65	39	R ¹ = R ² = R ⁴ = H; R ³ = CN
6d	86	51	58	40	69	63	R ¹ = R ² = R ⁴ = H; R ³ = CF ₃
6e	79	52	55	53	79	63	R ¹ = R ² = R ⁴ = H; R ³ = Me
6f	79	38	41	38	78	69	R ¹ = R ² = R ⁴ = H; R ³ = Cl
6g	74	51	74	51	76	56	R ¹ = R ² = R ⁴ = H; R ³ = Cl
6h	83	35	37	38	75	74	R ¹ = R ² = R ⁴ = H; R ³ = OMe
6i	78	46	56	47	72	62	R ¹ = R ² = R ⁴ = H; R ³ = OH
6j	55	59	59	65	74	44	R ¹ = R ² = R ⁴ = H; R ³ = F
6k	81	43	41	37	72	69	R ¹ = R ³ = R ⁴ = H; R ² = Me
6l	74	63	69	60	70	48	R ¹ = R ² = R ³ = R ⁴ = H

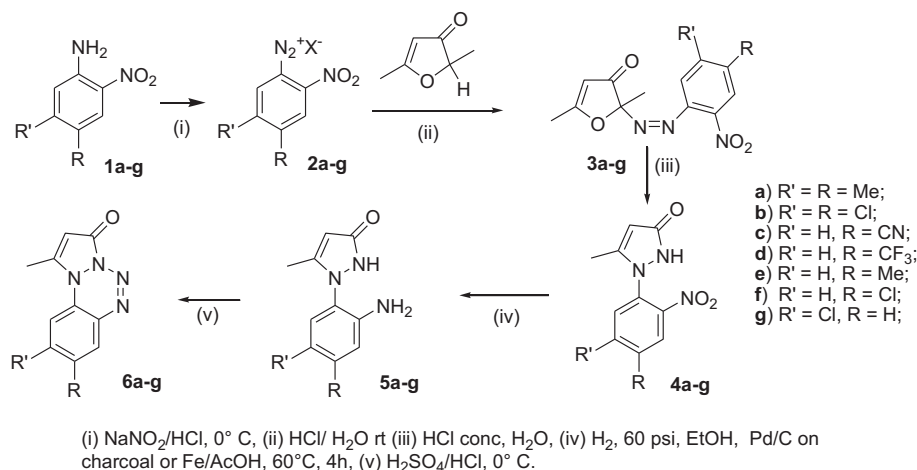
MA, mechanism of action: A%, percentage of affinity; A, Alkylating Agents; B, Antimetabolic Agents; C, Topoisomerase I Inhibitors; D, Topoisomerase II Inhibitors; E, RNA/DNA Antimetabolites; F, DNA Antimetabolites. Compounds 6e–l see Ref. [14].

comparison purposes, one included in the NCI panel (MCF-7, breast). Also for comparison reasons, three of the most active derivatives previously tested at the NCI Developmental Therapeutic Program (6e–6g) and four new PBT derivatives (6a–6d) are herein evaluated against these cell lines. The antiproliferative activity, expressed as IC₅₀ (μM), is listed in Table 2 (and graphically shown in Fig. 2).

An evaluation of these data point out that derivative 6d containing the –CF₃ in position 8 was active only toward 16HBE and LAN-5 cancer cell, in which a moderate and significant activity was observed at 30.9 and 15.1 μM, respectively. Interestingly, beside the strong electron withdrawing effect, the –CF₃ seems to amplify the valuable CNS tropism. Generally, according to literature data, the incorporation of fluorine into a drug increases the lipophilicity enhancing absorption into biological membranes [27].

Replacement of the latter group with the –CN, as in compound (6c), a strong withdrawing group, also possessing coordinating properties with metal ions, extended the activity to all the six tumor cell lines, but it remains moderate (IC₅₀ range 27–47 μM), probably due to the low solubility in the biological media. The introduction of a methyl group in the same position originating (6e), which resulted among the most active in the previous NCI screenings [14], appears to achieve promising results only against HeLa (IC₅₀ = 15.4 μM) and H292 (IC₅₀ = 25.1 μM), ineffective against LAN-5, whereas only moderately active toward the other cell lines. The addition of a second methyl group in the position 9, as in compound (6a) promoted a slight increase of the activity, especially against HeLa cell line, while no substantial variation is observed for the other ones. In parallel, in the case of the 8-chloro derivative (6f), and with respect to our panel of tumor cell lines, it was possible to evidence an increase of activity against the six lines tested, reaching a mean value of 22 μM. By adding another chlorine atom on position 9 of the PBT skeleton, compound (6b), the activity was enhanced as well as the selectivity toward MCF-7 and 16HBE (IC₅₀ 13.5 and 13.9 μM, respectively), while against the other cell lines the activity remained in the range 14.8–25.7 μM. In this latter case the effect of doubling the substituent corresponds to an increase of the activity, particularly toward MCF-7 and 16HBE, moderately for LAN-5, while derivative 6g, the 9-chloro substituted maintained a promising activity particularly toward HeLa cells.

Thus, nature and position of the different substituents in the PBT moiety affect the selectivity as well as the activity. The lipophilic character of chlorine and fluorine substituent enhances activity toward LAN-5 (CNS) with respect to the methyl group, conferring affinity to HeLa and H292 tumor cells.



Scheme 2. Reaction pathway.

2.3.2. In vitro NCI one dose screening

Beside the screening tests reported above against our panel of six cell lines, derivatives **6a–6d** were submitted to Development Therapeutics Program (DTP) NCI protocol. A single dose (10 μM) of the selected compounds was tested against a panel of approximately 60 tumor human cell lines grouped in nine disease sub-panels, including leukemia, non small-cell lung, colon, central nervous system, melanoma, ovarian, renal, prostate, and breast tumor cell lines [28–30].

Among the tested compounds, the 8,9-di-methyl derivative showed a selective activity against the Leukemia cell line CCRF-CEM and colon cancer cell line COLO 205, showing 81% and 45% growth inhibition (GI), respectively. The replacement of the two methyl groups with two chlorine atoms led to a valuable enhancement of the activity and selectivity against Colon Cancer (SW-620 and COLO 205) reaching the best result (G% = –64, meaning 64% of cell death), while toward Leukemia cell (CCRF-CEM) growth inhibition was maintained about 80%. Interestingly, although moderate, a significant growth inhibition (47%) against therapeutically refractory Non-Small Cell Lung Cancer (NCI-H522) was observed. This outcome, although could seem of modest entity, constitutes an interesting starting point for further developments for this refractory tumor disease (Table 3).

The most surprising results were the inactivity of the CN and CF_3 derivatives against all these cell lines. Only the di-methyl and di-chloro substituted derivatives resulted selectively effective toward some tumor cell lines, the two other derivatives were devoid

of interest. Based on the laboratory reactivity studies, if ring opening of the benzotetrazine ring is the rate determining step, a strong electron-withdrawing group should increase the biological activity. In the case of compounds **6c** and **6d**, although strong electron-withdrawing are present, the expected biological response was not observed. Probably, these data are not conclusive because of low solubility that could limit their efficacy.

2.3.3. Apoptosis induction

Apoptosis is endowed with a specific sequence of molecular events that culminates in cell death. Induction of apoptosis on cells can be promoted by different pathways. A number of methods are used to investigate apoptotic events. The key elements of the apoptotic pathway can involve typical membrane alterations, specific protease cascade, mitochondrial changes and DNA fragmentation. Because of some of these cell changes are not specific to the apoptotic process [31], in some cases different pathways could be strictly connected [32].

A peculiar cell event observed in the course of apoptosis is the mitochondrial membrane permeability alteration and apoptosis specific protease activators are released from mitochondria. By consequence the cytochrome C becomes redistributed to the cytosol, followed by subsequent depolarization of the inner mitochondrial membrane. The release of cytochrome C in the cytosol promotes caspase activation.

In our investigation, derivatives **6a–6g** have been evaluated on apoptotic induction against HeLa cell by flow cytometry analysis. The results, reported in Fig. 3 show the percentage of mitochondrial depolarization detected in the presence of PBT compounds at different concentrations with respect to staurosporine treated cells (positive control) and untreated cells (negative control).

As it can be observed, the –CN group on the PBT skeleton results ineffective for the activity (line **6c**) at least at concentration under 10 μM . Moving to the – CF_3 , possessing a strong electron withdrawing effect and lipophilic character, the activity profile does not appear dose dependent, even at low concentration (1 μM) the curve maintains constant, suggesting a saturation process (line **6d**). The replacement of the latter group in the same position of the ring with a methyl one, led to a better defined sigmoid curve showing the apoptotic induction in a range of 3–8 μM (line **6e**). The introduction of a second methyl group on the skeleton increases once more the activity, but reduced the range of activity to 3–4 μM (line **6a**). A similar trend, even more effective, is observed with the

Table 2
Antiproliferative activity (MTT) IC_{50}^a (μM).

	H292	HeLa	MCF-7	Caco-2	16-HBE	LAN-5
6a	23.4	13.2	46.7	46.8	38.9	95.5
6b	28.2	14.8	13.9	25.7	13.5	25.7
6c	43.6	27.0	35.9	37.1	46.7	28.2
6d	>100	>100	>100	>100	30.9	15.1
6e	25.1	15.4	42.6	50.2	36.3	93.3
6f	23.4	14.8	20.5	24.0	17.7	31.6
6g	25.1	15.8	29.5	34.6	27.5	48.9

^a IC_{50} : Concentration (μM) required to inhibit tumor cell proliferation by 50%. Antiproliferative activity was measured by MTT for cell viability according to the method described by Skehan and colleagues [26]. All measurements were performed in triplicate and each experiment was repeated at least three times. The IC_{50} value was calculated from the 50% formazan formation compared with a control without addition of drugs. Data are expressed as the mean \pm SE from the dose–response curves of at least three independent experiments.

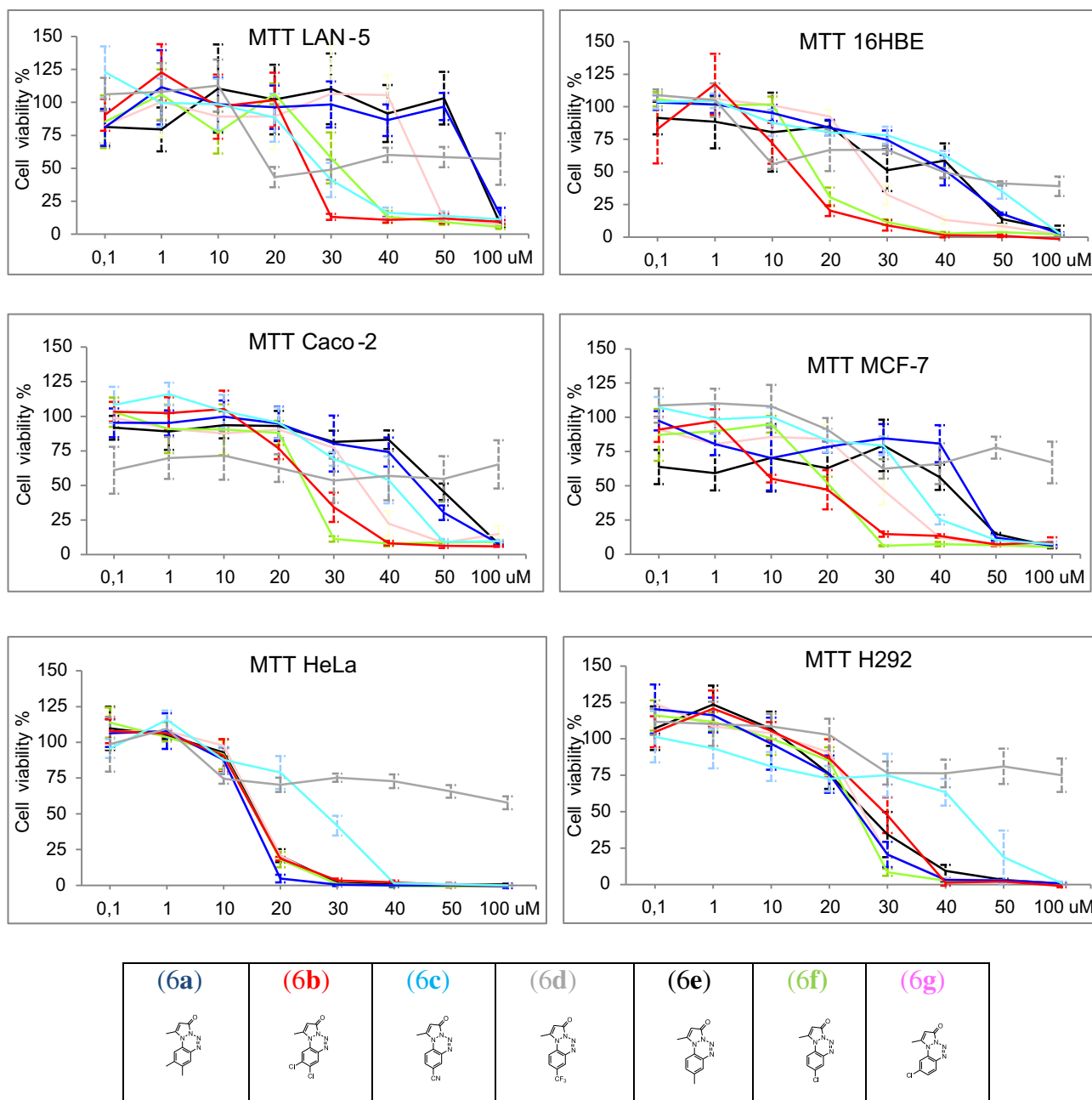


Fig. 2. Curve dose–response for PBT derivatives **6a–6g**. Data are means \pm SEM (Standard Error of the Mean) of triplicate determination.

chlorine substituted derivatives (line **6b** and **6f**), in this case the EC_{50} reaches 3 and 5 μ M, respectively.

2.3.4. Cell cycle analysis

To examine the influence of the more active compounds **6a–6b**, **6d**, on cell cycle distribution, the HeLa cells were exposed to four different concentrations of each compound for 72 h and, after incubation with propidium iodide as described in experimental section, the cells were evaluated using flow cytometry [38,39]. As shown in Fig. 4, when compared with the control, **6a**, **6b** (at 50 μ M) showed an increased sub-G₀/G₁ phase (cell death) of 18% and 25.4% and a S phase-specific effect of 10% and 19.4%, respectively. This S phase specificity suggests probable

interference with cellular DNA replication. Indeed, derivative **6d** induced a slight effect in the sub-G₀/G₁ phase and G₁ phase of 7.2% and –12%, respectively, but no variations in the other phases.

Since the order of efficacy in inducing cell death was: **6b** > **6a** > **6d** these results are in agreement with the trend observed in the anti-proliferative and apoptosis assays.

The S-phase checkpoint is involved with DNA repair and cell-cycle progression. It is known to react to DNA damage by reducing the rate of synthesis. Although it is still the least understood of the cellular checkpoints, recent studies on infrared-induced S-phase checkpoint activation have thrown valuable insight into its role in cancer development [33].

Table 3
Overview of the one dose NCI screening test results (G% for selected^a human tumor cell lines).

PANEL		6a	6b	6c	6d
Leukemia	CCRF-CeM	19	23	100	103
	MOLT-4	82	59	95	91
Non-Small Cell Lung Cancer	HOP-92	93	101	103	94
	NCI H522	97	54	97	97
Colon Cancer	Colo 205	66	-64	104	108
	SW 620	94	23	110	118
CNS Cancer	SNB 75	89	96	96	116
Melanoma	SK-MEL-2	96	102	99	99
Ovarian Cancer	IGROV-1	91	-	-	-
Renal Cancer	UO-31	84	81	105	84
Prostate Cancer	PC-3	100	94	101	101
Breast Cancer	T-47D	97	76	91	115

^a G% (Growth %). Data obtained from the NCI one dose mean graph. Interpretation of One-Dose Data: These data have been derived from the mean graph of the percent growth of treated cells. The number reported for the One-dose assay is growth relative to the no-drug control, and relative to the time zero number of cells. This allows detection of both growth inhibition (values between 0 and 100) and lethality (negative values, less than 0). For example, a value of 100 means no growth inhibition. A value of 40 would mean 60% growth inhibition. A value of 0 means no net growth over the course of the experiment. A value of -40 would mean 40% lethality. A value of -100 means all cells are dead (for more details see [Experimental](#)).

Although the attempts to correlate these biological assays needs yet to be clarified with deeper investigations, the analysis of the data arising from the *in silico* and the biological experiments performed, allow us to evidence some interesting results.

2.3.5. Biological data and VLAK protocol

As can be seen on [Table 1](#), except for derivative **6j**, the VLAK protocol classified seven of the first series of compounds (**6e–6l**) showing good percentage of affinity percent (A%) as alkylating agents (range 74–83%) coupled with a good A% as RNA/DNA antimetabolites (range 70–79%). Among the new synthesized compounds, the derivative **6d** (8-CF₃) even if it exhibited a valuable score value (86%) as alkylating candidate, in the HeLa cell cycle experiments, exhibited only a slight effect in the Sub G₀/G₁ and G₁ phase along with an interesting apoptosis induction without a dose dependent profile ([Fig. 3](#)). By contrast, an anti-proliferative activity

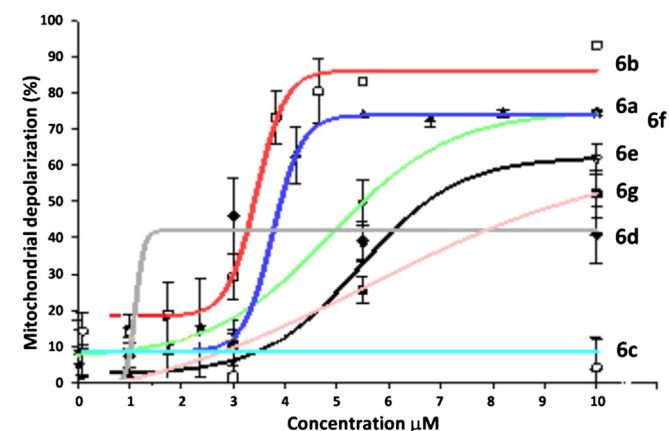


Fig. 3. Percentage of mitochondrial depolarization versus dose (μM). Experiments were performed in triplicates and replicated twice. The HeLa cells were seeded in 6 well flat-bottomed plates and incubated overnight with various drugs at serial concentrations. After treatment (for more details see [Experimental section](#)) cells were detached and analyzed using a FACSCalibur flow cytometer and the signal from TMRM was read on FL2. The data obtained were acquired, gated, compensated and analyzed using Cell-Quest Software. Mitochondrial depolarization analysis was measured by gating the cells treated overnight with $0.01 \mu\text{M}$ of staurosporine as positive control. Furthermore, the average signal of the negative control (untreated cells) was subtracted from the probe signal.

against LAN-5 (CNS) and 16HBE appeared, with IC₅₀ of 15 and 30 μM , respectively ([Table 2](#)).

Moving to the derivative **6c** (8-CN) also selected and synthesized for its good percentage of affinity as topoisomerase I and II inhibitor and antimetabolic agent ([Table 1](#)), it resulted poor in the apoptotic induction assays as well as on NCI one dose screening. It displayed only an anti-proliferative activity (MTT) in the range 27–28 μM on HeLa and LAN-5 cells. For these reasons the cell cycle test was not taken in consideration.

By contrast, improved results have been reached for the new designed derivative **6a** (8,9-dimethyl), classified as promising candidates as topoisomerase I/II inhibitor and RNA-DNA antimetabolite ([Table 1](#)). The anti-proliferative profile of the derivative **6a**, in the NCI tests ([Table 3](#)) performed at 10 μM one dose, displayed only a 20% of growth with respect to the control (untreated cell considered as 100% growth) reaching a IC₅₀ of 4 μM . Whereas in the antiproliferative MTT assays the more sensitive tumor cell line were the HeLa and the H292, displaying a IC₅₀ 13.2 and 23.4 μM , respectively. Interesting results in the range of 3–4 μM were found in the apoptosis induction. The assay has been carried out by comparison with the positive control ($0.01 \mu\text{M}$ staurosporine) and the negative control (the untreated cells). Toward the cell cycle on Sub G₀/G₁ phase, a cell death of 18% was observed along with 10% of S phase specific effect. It is worthy to note, that in this phase the topoisomerase I as well as RNA-DNA antimetabolites acts according to the classification suggested by the VLAK protocol.

The best results have been obtained with derivative **6b** (8,9-dichloro), which was classified as antimetabolic agents (A% = 90) and as topoisomerase II inhibitors (A% = 79). With respect to the antiproliferative activity, either in the MTT test and in the one dose NCI screening, some selective interesting results were obtained. In the MTT assays ([Table 2](#)), HeLa and MCF-7 cells resulted as the more sensitive (IC₅₀ 14.8 and 13.9 μM). Especially for MCF-7, when the mono-chlorinated **6f** was compared with the related dichloro one **6b**, an increased of potency of nearly two folds was observed, moving from 20.5 to 13.9 μM . In this case, the high A% (90) value as antimetabolic agent and as topoisomerase II inhibitor (79%), matches well with the best biological outcomes.

Also of interest are the results of the NCI one dose (10 μM) testing. In [Table 3](#) some representative data are therein reported. Leukemia cell (CCRF-CeM) showed a growth (G%) of 23% (77% of inhibition with respect to the untreated cell used as control). The most sensitive was the colon tumor cell line (Colo205) exhibiting 64% of cell death. For this last tumor cell line the potency of **6b** is the highest. Although less sensitive than the previous one, other colon tumor cell line is the SW 620 which showed only a G% = 23%.

Associated to these selective valuable anti-proliferative activity, the derivative **6b** exhibits the best result either on apoptosis induction (EC₅₀ = 3.5 μM) and on the cell cycle showing an effect on Sub G₀/G₁ phase of 25% along with a 19% on S phase as compared with control.

In our study, the results achieved in the case of the new designed and synthesized compounds **6a–6d**, it can be observed that only the 8,9 dimethyl (**6a**) and the 8,9-dichloro derivatives (**6b**) have been improved on their efficacy, while for the 8-CN (**6c**) and derivatives 8-CF₃ (**6d**) the expected activity increases were not evidenced or only partially noticed.

3. Conclusions

For the optimization of the PBT derivatives an in house database (a library of PBT derivatives) was built and on which the VLAK protocol has been applied.

Based on the main role played by the introduction of suitable functionalities onto the PBT skeleton able to modulate the reactivity

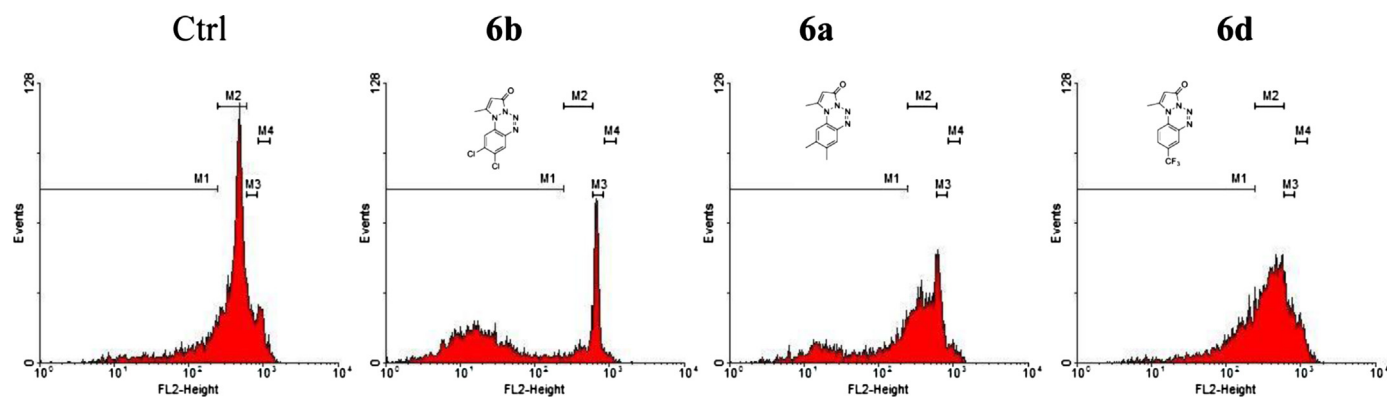


Fig. 4. Flow cytometry profile of the more active compounds. Cells from each sample were analyzed using a FACSCalibur supported with CellQuest acquisition and data analysis were made by comparison with the untreated cells, used as control. The effect of the DMSO were also subtracted [38,39].

as well as the selectivity toward cell lines, we selected from our in house built database, new derivatives so as to potentiate the effects exerted by the groups which resulted among the more influent in modulating the activity in the previous SAR studies (**6a**, **6b**) and new derivatives so as to increase the electron withdrawing effect on the “C” tricyclic moiety (**6c**, **6d**) to get some insight regarding in chemical reactivity and biological activity.

Compared to the mono-substituted methyl and chlorine derivatives (**6e**, **6f**), the doubling of the substituent resulted beneficial for the activity, in agreement with the affinity percentage shown on Table 1. By contrast, in the case of $-\text{CN}$ and $-\text{CF}_3$ groups (**6c**, **6d**), the expected improvements of activity were not achieved despite good prediction arisen from our virtual lock and key protocol.

The order of potency of the active compound followed the same trend either in the evaluation of apoptosis induction and in the viability test. In all the tests, the activity order observed was derivative **6b** > **6a** > **6f** > **6e** > **6g** > **6d** > **6c**. Curiously, this trend is mirrored by the solubility scale (from the more to the less one).

The cell cycle data support probable interference of these compounds with DNA replication, the main event in phase S. The similar trend, in terms of order of activity exhibited by the compounds in the different assays, suggests that the observed anti-proliferative activity is probably exerted through apoptosis induction and cell cycle arrest in the S phase, as typical for alkylating agents.

Thus, although a lot of work still remain to make light on, a promising new class of valuable apoptotic inducers having a PBT scaffold is proposed herein. Further developments with properly designed group conferring enhanced solubility properties could help to clarify these premises.

4. Experimental

4.1. VLAK protocol

The compounds contained in the NCI AntiCancer Agents Mechanism (NCI ACAM) [24,25,29] and those in the PBT databases, were drawn and optimized *in vacuo* by ligprep of MAESTRO SUITE [34]. The NCI ACAM Database entries containing cations or consisting of a mix of two structures were excluded. Thus the starting database was constituted from 114 compounds classified in six mechanism of action: 30, Alkylating Agents; 13, Antimitotic Agents; 24, Topoisomerase I Inhibitors; 15, Topoisomerase II Inhibitors; 16, RNA/DNA Antimetabolites; 16, DNA Antimetabolites (Supplementary material). CODESSA PRO software was used for the molecular descriptors calculation [35]. For all structures 286 molecular

descriptor belonging to different classes were calculated (Supplementary material).

Thus, for each class of drugs (Alkylating Agents, Antimitotic Agents, Topoisomerase I Inhibitors, Topoisomerase II Inhibitors, RNA/DNA Antimetabolites, and DNA Antimetabolites), a “lock model” was generated starting from own known drugs.

In particular, for each class of drugs with known mechanism of action (MA) (Fig. 5a), the lock model is defined as a sequence of molecular descriptor value ranges. Each range is defined as $\mu\text{Dj}(\text{MA}) \pm \sigma\text{Dj}(\text{MA})$, where $\mu\text{Dj}(\text{MA})$ is the molecular descriptor average value and $\sigma\text{Dj}(\text{MA})$ is the standard deviation (Fig. 5b, Supplementary material).

When the molecular descriptor value Dj of a tested structure X (Fig. 5c) falls within the defined range ($\mu\text{Dj} \pm \sigma\text{Dj}$) $\alpha = 1$ (ie D1, D3, and Dj), otherwise $\alpha = 0$ (ie D2, D4) (Fig. 5d). At the end each *in house* database structure is converted in a binary sequence. In the proposed protocol, it is supposed that the higher is the number of fitted pins, the higher will be the potential anticancer capability of the investigated compound. Thus, the percentage of affinity $A\%$ (eq. (1)) for each compound belonging to *in house* database was defined for each class (MA) as:

$$A\% = \sum \alpha_{i,j}(\text{MA}) / D_{\text{tot}} * 100 \quad (1)$$

where $\sum \alpha_{i,j}(\text{MA})$ is the sum of all fitted molecular descriptors for the MA class and D_{tot} is the total of the molecular descriptors used in the VLAK protocol.

In Supplementary material are reported the output results for the selected PBTs related the lock models representing each class of drugs (MAs).

4.2. Chemistry

4.2.1. Material and methods

All melting points were taken on a Sanyo-Gallenkamp capillary apparatus and are uncorrected; IR spectra were recorded with bromoform on NaCl window with a Jasco FT/IR 5300 spectrophotometer; ^1H and ^{13}C NMR spectra were recorded in CDCl_3 or DMSO- d_6 solution as below specified, using a Bruker AC-E series 200 MHz spectrometer, unless otherwise specified. As internal reference residual peak of the solvent was calibrated, at δ 7.26 and 2.50 ppm, respectively for CDCl_3 and DMSO- d_6 . Mass spectroscopy was performed using a GC-MS Shimadzu QP5050 with EI (75eV). Column chromatography was performed with Merck silica gel 230–400 Mesh ASTM. Thin layer chromatography was performed on pre-coated (0.25 mm) silica gel GF $_{254}$ plates; compounds were detected

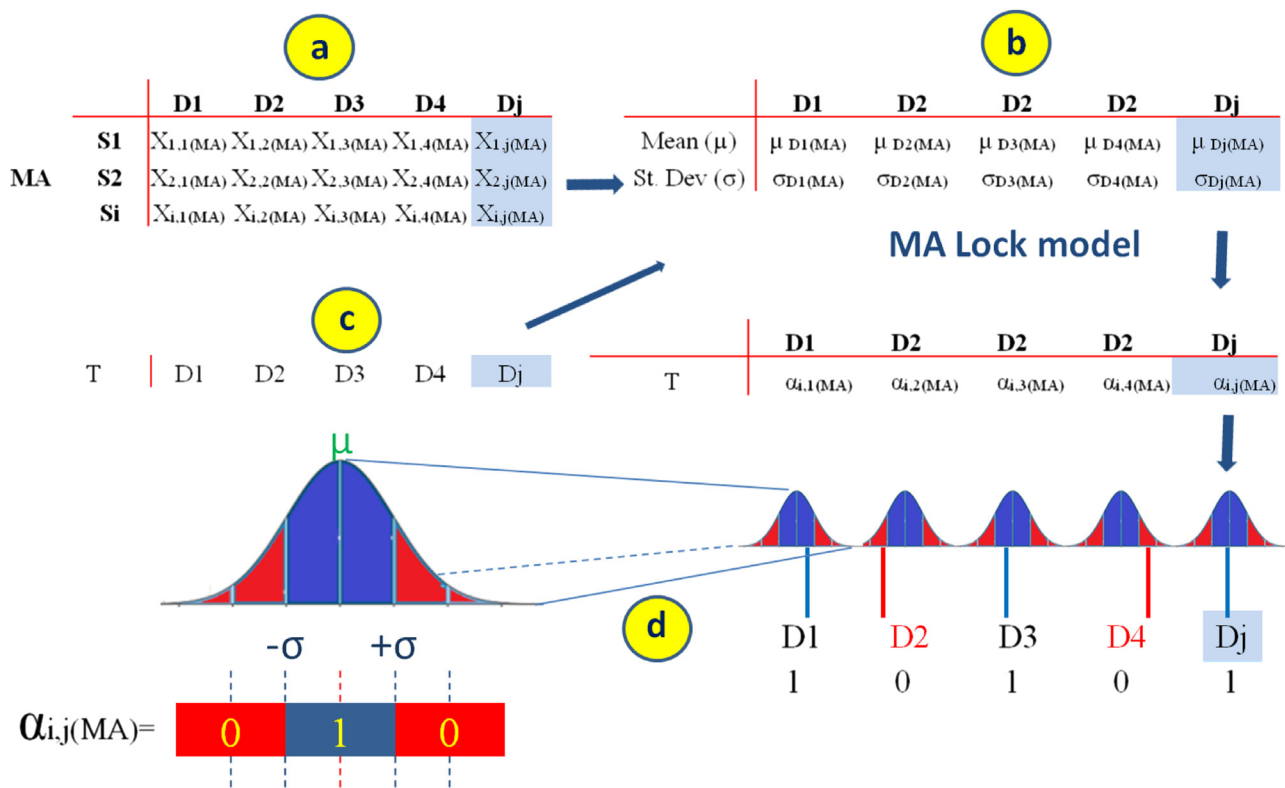


Fig. 5. Vlak protocol applied on NCI ACAM database. MA, mechanism of action; Dj, molecular descriptors; Si, structures; T, *in silico* screened entry.

with 254 nm UV lamp. Microanalyses were in agreement with theoretical values $\pm 0.4\%$.

4.2.2. General procedure for the preparation of 2,5-dimethyl-2-(2-nitroarylazo)-3-oxo-2,3-dihydrofurans 3a–g

To a suspension of 2-Nitroanilines **2a–2g** (10 mmol) in water (5 mL) and hydrochloric acid (37%, 2.5 mL), a solution of sodium nitrite (0.74 g, 10.75 mmol) in water (4 mL) at 0 °C was added dropwise. The mixture was stirred for 1 h, diluted with water (30 mL) and made acid with concentrated hydrochloric acid (2 mL). In the case of **2b,f** the reactions were carried out at room temperature. To this solution, freshly distilled 2,5-dimethyl-3-oxo-2,3-dihydrofuran [36] (1.24 g, 11 mmol) was added and the mixture was stirred for 1 h at room temperature. The crude residue was collected by filtration. After drying, it was purified by column chromatography using a dichloromethane/ethyl acetate mixture in gradient as eluent and recrystallized from ethanol.

4.2.2.1. 2,5-Dimethyl-2-(4,5-dimethyl-2-nitrophenylazo)-3-oxo-2,3-dihydrofuran (3a). Yield 95%. Mp 93 °C. IR: 1717 (CO), 1539 and 1321 (NO₂) cm⁻¹. ¹H NMR: δ (DMSO) 1.61 (s, 3H, CH₃), 2.33 (s, 3H, CH₃), 2.36 (s, 3H, CH₃), 2.44 (s, 3H, CH₃), 5.80 (s, 1H, H₄), 7.10 (s, 1H, H_{3'}), 7.94 (s, 1H, H_{6'}). ¹³C NMR: δ (DMSO) 16.64 (CH₃), 18.21 (CH₃), 19.06 (CH₃), 19.23 (CH₃), 102.67 (CH), 107.44 (C), 118.50 (CH), 124.70 (CH), 141.51 (C), 141.53 (C), 143.92 (C), 143.94 (C), 191.55 (C), 194.92 (CO). M/z (EI) 151 (M⁺ – 139, 100%), 135, 806), 121 (22), 105 (72) and 177 (M⁺ – 111, 100%), 162 (17), 148 (10), 132 (21), 119 (98), 103 (18), 91 (28). Anal. Calcd. For C, 58.13; H, 5.23; N, 14.53. Found: C, 58.17; H, 5.19; N, 14.47.

4.2.2.2. 2-(4,5-Dichloro-2-nitrophenylazo)-2,5-dimethyl-3-oxo-2,3-dihydrofuran (3b). Yield 78%. Mp 140–141 °C. IR: 1715 (CO), 1532

and 1341 (NO₂), 934 and 897 (C–Cl) cm⁻¹. ¹H NMR: δ (DMSO) 1.63 (s, 3H, CH₃), 2.45 (s, 3H, CH₃), 5.82 (s, 1H, H₄), 7.64 (s, 1H, H_{6'}), 8.59 (s, 1H, H_{3'}). ¹³C NMR: δ (DMSO) 16.65 (CH₃), 18.46 (CH₃), 102.63 (CH), 107.76 (C), 120.26 (CH), 126.47 (CH), 134.25 (C), 136.99 (C), 142.28 (C), 144.67 (C), 191.66 (C), 194.14 (CO). M/z (EI) 191 (M⁺ – 139, 84%), 193 (M⁺ – 137, 54%), 175 (5), 177 (3), 161 (36), 163 (23), 145 (99), 147 (64), 133 (51), 135 (30), 109 (100), 111 (31) and 217 (M⁺ – 113, 50%), 219 (35), 202 (13), 204 (7), 172 (9), 174 (6), 161 (35), 163 (16). Anal. Calcd. For C, 43.66; H, 2.75; Cl, 21.48; N, 12.73. Found: C, 43.70; H, 2.71; N, 12.78.

4.2.2.3. 2-(4-Cyano-2-nitrophenylazo)-2,5-dimethyl-3-oxo-2,3-dihydrofuran (3c). Yield 85%. Mp 89–90 °C. IR: 1715 (CO), 1539 and 1348 (NO₂) cm⁻¹. ¹H NMR δ (DMSO) 1.66 (s, 3H, CH₃), 2.46 (s, 3H, CH₃), 5.83 (s, 1H, H₄), 7.46 (d, 1H, J = 7.3 Hz, H_{6'}), 8.28 (dd, 1H, J = 7.3, 1.3 Hz, H_{5'}), 8.79 (d, 1H, J = 1.3 Hz, H_{3'}). ¹³C NMR: δ (DMSO) 16.63 (CH₃), 18.36 (CH₃), 102.64 (CH), 108.04 (C), 114.07 (C), 116.43 (CN) 120.20 (CH), 128.92 (CH), 138.23 (CH), 145.21 (C), 145.94 (C), 186.35 (C), 188.54 (CO). M/z (EI) 148 (M⁺ – 138, 49%), 132 (3), 118 (5), 102 (100), 90 (14), 75 (38) and 174 (M⁺ – 112, 46%), 159 (20), 140 (21), 129 (8), 116 (37), 102, (17), 91 (19) and 226 (M⁺ – 40, 10%), 211 (46), 171 (5), 155 (4), 118 (3), 111 (2), 86 (3). Anal. Calcd. For C, 54.55; H, 3.52; N, 19.57. Found: C, 54.60; H, 3.49; N, 19.51.

4.2.2.4. 2,5-Dimethyl-2-(2-nitrophenylazo-4-trifluoromethyl)-3-oxo-2,3-dihydrofuran (3d). Yield 79%. Mp 108 °C. IR: 1717 (CO), 1539 and 1262 (NO₂) cm⁻¹. ¹H NMR δ (DMSO) 1.67 (s, 3H, CH₃), 2.47 (s, 3H, CH₃), 5.85 (s, 1H, H₄), 7.52 (d, 1H, J = 7.8 Hz, H_{6'}), 7.69 (dd, 1H, J = 7.8, 1.2 Hz, H_{5'}), 8.61 (d, 1H, J = 1.2 Hz, H_{3'}). ¹³C NMR: δ (DMSO) 16.63 (CH₃), 18.32 (CH₃), 102.66 (CH), 107.98 (C), 122.59 (q, J = 272.8 Hz, CF₃), 120.33 (CH), 122.22 (q, J = 3.7 Hz, CH), 131.30 (q, J = 33.3 Hz, C), 131.13 (q, J = 3.2 Hz, CH), 145.62 (C), 145.86 (C), 191.80 (C), 194.08

(CO). M/z (EI) 198 ($M^+ - 131$), 222 ($M^+ - 107$), 269 ($M^+ - 60$). Anal. Calcd. For C, 47.43; H, 3.06; F, 17.31; N, 12.76. Found: C, 47.38; H, 3.03; F, 17.35; N, 12.72.

Compounds **3e–g** were identical to literature report [14].

4.2.3. General method for the preparation of 5-methyl-1-(2-nitroaryl)-pyrazol-3-ones **4a–g**

To a concentrated hydrochloric acid solution (37%, 7 mL), 2-(Arylazo)-2,5-dimethyl-3-oxo-2,3-dihydrofuran **3a–3g** (10 mmol) was added in small portions with stirring, while care is taken that the temperature of the mixture does not exceed 30 °C. After the addition was complete the stirred mixture is kept at 20–30 °C, usually for 1 h. The cooled mixture was then poured onto ice water and made basic with 30% aqueous sodium hydroxide. It was then diluted with water to complete dissolution of the sodium salt of the pyrazolone. The resultant solution was extracted with diethyl ether (3 × 100 mL). The aqueous phase was made acid with diluted hydrochloric acid, with stirring and cooling to precipitate the product. The solid was isolated by filtration, washed with water, air dried and recrystallized from ethanol [37].

4.2.3.1. 1-(4,5-Dimethyl-2-nitrophenyl)-5-methyl-1,2-dihydropyrazol-3-one (**4a**). Yield 96%. Mp 235 °C. IR: 3195 (NH), 1524 and 1350 (NO₂) cm⁻¹. ¹H NMR: δ (DMSO) 2.12 (s, 3H, CH₃), 2.34 (s, 6H, 2xCH₃), 5.58 (s, 1H, H₄), 7.47 (s, 1H, H₃), 7.83 (s, 1H, H₆), 9.90 (s, 1H, NH, exchangeable with D₂O). ¹³C NMR: δ (DMSO) 11.49 (CH₃), 18.73 (CH₃), 19.22 (CH₃), 93.19 (CH), 125.30 (CH), 129.38 (CH), 129.80 (C), 137.98 (C), 140.85 (C), 143.32 (C), 143.67 (C), 161.93 (CO). M/z: (EI) 287 ($M^+ 45\%$), 289 ($M^+ + 2, 45\%$), 270 (17), 252 (9), 171 (17), 157 (20), 145 (17), 109 (20), 97 (100), 85 (33). Anal. Calcd. For C, 58.29; H, 5.30; N, 16.99. Found: C, 58.25; H, 5.32; N, 17.02.

4.2.3.2. 1-(4,5-Dichloro-2-nitrophenyl)-5-methylpyrazol-3-one (**4b**). Yield 89%. Mp 220 °C. IR: 3104 (OH), 1530 and 1345 (NO₂), 909 (C–Cl) cm⁻¹. ¹H NMR: δ (DMSO) 2.23 (s, 3H, CH₃), 5.66 (s, 1H, H₄), 8.19 (s, 1H, H₅), 8.44 (s, 1H, H₃), 10.11 (s, 1H, NH). ¹³C NMR: δ (DMSO) 11.38 (CH₃), 94.63 (CH), 126.70 (CH), 129.53 (CH), 130.83 (C), 131.55 (C), 135.78 (C), 141.65 (C), 144.54 (C), 162.59 (CO). M/z (EI) ($M^+ 287, 45\%$), 289 ($M^+ + 2, 31\%$), 270 (16), 272 (4), 252 (7), 254 (3), 222 (6), 224 (2), 171 (18), 158 (20), 160 (15), 145 (17), 147 (10), 109 (20), 111 (13), 97 (100). Anal. Calcd. For C, 41.69; H, 2.45; Cl, 24.61; N, 14.59. Found: C, 41.71; H, 2.43; Cl, 24.58; N, 14.56.

4.2.3.3. 1-(4-Cyano-2-nitrophenyl)-5-methylpyrazol-3-one (**4c**). Yield 75%. Mp 217 °C. IR: 3445 (NH), 1694 (CO), 1541 e 1354 (NO₂); 2257 (CN) cm⁻¹. ¹H NMR: δ (DMSO) 2.22 (s, 3H, CH₃), 5.67 (s, 1H, H₄), 7.83 (d, 1H, *J* = 8.3 Hz, H₆), 8.23 (dd, 1H, *J* = 8.3, 1.9 Hz, H₅), 8.42 (d, 1H, *J* = 1.9 Hz, H₃), 10.14 (s, 1H, NH). ¹³C NMR: δ (DMSO) 11.70 (CH₃), 94.79 (CH), 124.17 (CH), 128.05 (CH), 131.97 (CH), 133.86 (CN), 134.03 (C), 141.24 (C), 145.26 (C), 162.57 (C), 166.06 (CO). Anal. Calcd. For C, 54.10; H, 3.30; N, 22.94. Found: C, 54.1; H, 3.28; N, 22.96.

4.2.3.4. 1-(2-Nitrophenyl-4-trifluoromethyl)-5-methylpyrazol-3-one (**4d**). Yield 85%. Mp 218 °C. IR: 3150 (NH), 1631 (CO), 1545 and 1354 (NO₂), 1325 (CF₃) cm⁻¹. ¹H NMR: δ (DMSO) 2.26 (s, 3H, CH₃), 5.71 (s, 1H, H₄), 7.97 (dd, 1H, *J* = 7.4, 1.4 Hz, H₆), 8.17 (dd, 1H, *J* = 7.4, 1.4 Hz, H₅), 8.44 (d, 1H, *J* = 1.4 Hz, H₃), 10.20 (1H, s, NH). ¹³C NMR: δ (DMSO) 11.57 (CH₃), 95.28 (CH), 122.79 (q, *J* = 272 Hz, CF₃), 122.64 (q, *J* = 3.7 Hz, CH), 128.15 (q, *J* = 33.9 Hz, C₄'), 128.86 (d, C₆'), 129.93 (q, *J* = 3.7 Hz, CH), 135.05 (s, C₁'), 141.47 (s, C₅), 145.61 (s, C₂'), 162.82 (CO). M/z (EI) 287 ($M^+, 100\%$), 270 (27), 257 (12), 239 (7), 228 (8), 212 (12), 198 (16), 186 (14), 172 (11), 158 (12), 145 (48), 126 (18), 115 (17), 97 (98), 85 (31), 69 (23). Anal. Calcd. For C, 46.00; H, 2.81; F, 19.85; N, 14.63. Found: C, 45.97; H, 2.83; N, 14.66.

Compounds **4e–g** were identical to literature [14].

4.2.4. General procedure for the preparation of: 1-(2-aminoaryl)-5-methylpyrazol-3-ones **5a–g**

Method A: A solution of nitro derivatives **4a, 4c–4d** (42 mmol) was reduced overnight over 10% Pd on charcoal in ethanol in a Parr apparatus at 50 psi at room temperature. Removal of the catalyst and evaporation of the solvent under reduced pressure gave a residue which was purified by flash chromatography using a dichloromethane/ethyl acetate mixture in gradient as eluent and recrystallized from ethanol.

4.2.4.1. 1-(2-Aminophenyl)-4,5-dimethylpyrazol-3-one (**5a**). Yield 98%. Mp 220–222 °C. IR: 3439 and 3360 (NH₂), 3100 (OH), cm⁻¹. ¹H NMR: δ (300 MHz DMSO) 1.99 (s, 3H, CH₃), 2.07 (s, 3H, CH₃), 2.12 (s, 3H, CH₃), 4.61 (2H, s, NH₂, exchangeable), 5.47 (s, 1H, H₄), 6.60 (s, 1H, H₆'), 6.76 (s, 1H, H₃'), 9.72 (bs, 1H, NH, exchangeable). ¹³C NMR: δ (75 MHz DMSO) 11.60 (CH₃), 18.26 (CH₃), 19.34 (CH₃), 91.23 (CH), 117.22 (CH), 122.28 (C), 123.66 (CH), 128.10 (CH), 136.67 (C), 140.46 (C), 142.09 (C), 161.12 (CO). M/z (EI) 217 ($M^+, 100\%$), 202 (10), 185 (06), 173 (39), 159 (20), 147 (20), 135 (15), 120 (07), 108 (08). Anal. Calcd. For C, 66.34; H, 6.96; N, 19.34. Found: C, 66.39; H, 7.00; N, 19.31.

4.2.4.2. 1-(2-Amino-4-cyanophenyl)-5-methylpyrazol-3-one (**5c**). Yield 75%. Mp 205 °C. IR: 3483 (NH) 3396 and 3210 (NH₂), 3140 (OH), 2226 (CN), cm⁻¹. ¹H NMR: δ (DMSO/CDCl₃) δ: 2.05 (s, 3H, CH₃), 5.26 (s, 2H, NH₂), 5.49 (s, 1H, H₄), 6.85 (dd, 1H, *J* = 8.0, 1.2 Hz, H₅), 7.03 (d, 1H, *J* = 8.0 Hz, H₆'), 7.08 (d, 1H, *J* = 1.2 Hz, H₃'), 9.69 (s, 1H, NH). ¹³C NMR: δ (DMSO/CDCl₃) 11.42 (CH₃), 92.39 (CH), 110.97 (C), 118.31 (CN), 118.60 (CH), 118.79 (CH), 127.25 (CH), 127.38 (C), 140.51 (C), 144.59 (C), 161.73 (CO). M/z (EI) 214 ($M^+, 45\%$), 170 (20), 144 (19), 117 (23), 84 (31). Anal. Calcd. For C, 61.67; H, 4.71; N, 26.15. Found: C, 61.71; H, 4.68; N, 26.12.

4.2.4.3. 1-(2-Amino-4-trifluoromethylphenyl)-5-methylpyrazol-3-one (**5d**). Yield 80%. Mp 216 °C. IR: 3478 and 3358 (NH₂), 3200 (OH), 1344 (CF₃) cm⁻¹. ¹H NMR: δ (250 MHz, CDCl₃) 2.09 (s, 3H, CH₃), 5.59 (s, 1H, H₄), 5.9–6.3 (bs, 2H, NH₂), 7.01 (dd, 1H, *J* = 7.8, 0.8 Hz, H₆'), 7.05 (d, 1H, *J* = 0.8 Hz, H₃'), 7.18 (d, 1H, *J* = 7.8 Hz, H₅'), 7.28 (bs, 1H, NH). ¹³C NMR: δ (63 MHz, CDCl₃) 11.55 (CH₃), 92.76 (CH), 113.36 (q, *J* = 3.7 Hz, C₃'), 114.72 (q, *J* = 3.7 Hz, C₅'), 126.38 (q, *J* = 272 Hz, CF₃), 126.35 (C₁'), 128.80 (C₆'), 132.08 (q, *J* = 31.4 Hz, C₄'), 142.88 (C₂'), 144.00 (C₅), 163.41 (CO). M/z (EI) 257 ($M^+, 100\%$), 239 (12), 213 (28), 199 (22), 187 (21), 175 (15), 160 (16), 140 (12). Anal. Calcd. For C, 51.37; H, 3.92; F, 22.16; N, 16.34. Found: C, 51.40; H, 3.89; F, 22.19; N, 16.29.

4.2.5. Method B

Iron powder (670 mg, 12 mmol) was added to a solution of **5b** (3.4 mmol) in acetic acid (30 mL). The mixture was kept at 60 °C in a steam bath for 24 h. The reaction mixture was cooled, poured onto crushed ice and extracted with dichloromethane. The organic layer, dried over sodium sulfate and evaporated under reduced pressure, gave a residue which was purified by chromatography and recrystallization from ethanol.

4.2.5.1. 1-(2-Amino-4,5-dichlorophenyl)-5-methylpyrazol-3-one (**5b**). Yield 82%. Mp 246 °C. IR: 3605 (OH), 3455 and 3355 (NH₂), 1624 (CO), 927 (C–Cl) cm⁻¹; ¹H NMR: δ (DMSO) 2.05 (s, 3H, CH₃), 5.43 (s, 2H, NH₂), 5.55 (s, 1H, H₄), 7.02 (s, 1H, H₆'), 7.30 (s, 1H, H₃'), 9.91 (s, 1H, NH). ¹³C NMR: δ (DMSO) 11.32 (CH₃), 92.24 (CH), 115.85 (C), 115.99 (CH), 123.70 (C), 128.65 (CH), 130.68 (C), 141.01 (C), 144.85 (C), 161.58 (CO). M/z (EI) 257 ($M^+ 100$), 259 ($M^+ + 2, 70\%$), 215 (41), 199 (29), 178 (24), 133 (40), 108 (23). Anal. Calcd. For C, 46.53;

H, 3.51; Cl, 27.47; N, 16.28. Found: C, 46.57; H, 3.49; Cl, 27.51; N, 16.30.

Compounds **5e–g** were identical to literature [14].

4.2.6. General method for the preparation of 1-methyl-8,9-substituted-3H-pyrazolo[1,2-a]benzotetrazin-3-ones **6a–6g**

Concentrated sulfuric acid (0.4 mL) was added to a solution of **5a–5g**, (1.9 mmol) in water (10 mL) and the mixture was diazotized with sodium nitrite (145 mg, 2.1 mmol) in water (10 mL) at 0 °C. The reactants were stirred for further 2 h at room temperature, and then were kept at 60 °C for 3 h. The mixture was cooled to room temperature, and made basic with solid sodium carbonate. The solid precipitate was filtered off, and air dried.

4.2.6.1. 1,8,9-Trimethyl-3H-pyrazolo[1,2-a]benzotetrazin-3-one (6a). Yield 81%. Mp 142–143 °C (dec.). IR: 1678 (CO) cm^{-1} . ^1H NMR: δ (DMSO) 2.24 (s, 3H, CH₃), 2.30 (s, 3H, CH₃), 2.63 (s, 3H, CH₃), 5.45 (s, 1H, H₂), 7.26 (s, 1H, H₁₀), 7.51 (s, 1H, H₇). ^{13}C NMR: δ (DMSO) 14.84 (CH₃), 18.99 (CH₃), 20.06 (CH₃), 95.61 (CH), 113.96 (CH), 122.29 (CH), 125.21 (C), 129.30 (C), 136.27 (C), 137.35 (C), 144.53 (C), 161.51 (CO). Anal. Calcd. For C, 63.15; H, 5.30; N, 24.55. Found: C, 62.99; H, 5.15; N, 24.45.

4.2.6.2. 8,9-Dichloro-1-methyl-3H-pyrazolo[1,2-a]benzotetrazin-3-one (6b). Yield 73%. Mp 143 °C (dec.). IR: 1676 (CO), 926 (C–Cl) cm^{-1} . ^1H NMR: δ (250 MHz, CDCl₃) 2.64 (s, 3H, CH₃), 5.61 (s, 1H, H₂), 7.34 (s, 1H, H₁₀), 7.86 (s, 1H, H₇). ^{13}C NMR: δ (50 MHz, CDCl₃) 15.52 (CH₃), 96.86 (CH), 113.76 (CH), 126.86 (C), 127.76 (C), 129.75 (C), 131.03 (CH), 137.94 (C), 143.47 (C), 156.90 (CO). M/z (EI) 212 (M⁺ – 57, 100%), 214 (81), 185 (65), 187 (46); 144 (27), 146 (23), 111 (8), 109 (20). Anal. Calcd. For C, 44.64; H, 2.25; Cl, 26.35; N, 20.82. Found: C, 44.71; H, 2.31; Cl, 26.42; N, 20.70.

4.2.6.3. 8-Cyano-1-methyl-3H-pyrazolo[1,2-a]benzotetrazin-3-One (6c). Yield 67%. Mp 176–178 °C (dec.). IR: 1697 (CO) cm^{-1} . ^1H NMR: δ (250 MHz, DMSO) 2.63 (s, 3H, CH₃), 5.75 (s, 1H, H), 7.59 (d, 1H, J = 8.7 Hz, H₁₀), 7.98 (dd, 1H, J = 8.7, 1.9 Hz, H₉), 8.27 (d, 1H, J = 1.9 Hz, H₇). ^{13}C NMR: δ (50 MHz, DMSO) 14.80 (CH₃), 96.26 (CH), 107.16 (C), 114.04 (C), 117.62 (CN), 132.14 (CH), 132.75 (C), 137.85 (CH), 145.47 (C), 159.97 (C), 163.82 (CO). Anal. Calcd. For C, 58.67; H, 3.13; N, 31.10. Found: C, 58.81; H, 2.99; N, 31.25.

4.2.6.4. 8-Trifluoromethyl-1-methyl-3H-pyrazolo[1,2-a]benzotetrazin-3-One (6d). Yield 77%. Mp 237–238 °C (dec.). IR: 1699 (CO), 983 (CF₃) cm^{-1} . ^1H NMR: δ (250 MHz, DMSO) 2.04 (s, 3H, CH₃), 5.56 (s, 1H, H₂), 7.57 (s, 2H, H₇ and H₉), 7.83 (s, 1H, H₁₀). ^{13}C NMR: δ (50 MHz, DMSO) 14.61 (CH₃), 106.68 (CH), 118.85 (CH), 119.75 (CH), 124.14 (q, J = 270 Hz, CF₃), 128.81 (q, J = 32 Hz, C), 130.98 (C), 132.19 (CH), 135.22 (C), 147.83 (C), 166.91 (CO). Anal. Calcd. For C, 49.26; H, 2.63; F, 21.25; N, 20.89. Found: C, 49.40; H, 2.61; F, 21.29; N, 20.81.

Compounds **6e–g** were identical to literature report [14].

4.3. Biology

4.3.1. NCI protocol (DTP program) methodology of the *in vitro* cancer screen [30]

The human tumor cell lines of the cancer screening panel are grown in RPMI 1640 medium containing 5% fetal bovine serum and 2 mM L-glutamine. For a typical screening experiment, cells are inoculated into 96 well microtiter plates in 100 μL at plating densities ranging from 5000 to 40,000 cells/well depending on the doubling time of individual cell lines. After cell inoculation, the microtiter plates are incubated at 37 °C, 5% CO₂, 95% air and 100% relative humidity for 24 h prior to addition of experimental drugs.

After 24 h, two plates of each cell line are fixed *in situ* with TCA, to represent a measurement of the cell population for each cell line at the time of drug addition (Tz). Experimental drugs are solubilized in dimethyl sulfoxide at 400-fold the desired final maximum test concentration and stored frozen prior to use. At the time of drug addition, an aliquot of frozen concentrate is thawed and diluted to twice the desired final maximum test concentration with complete medium containing 50 $\mu\text{g}/\text{ml}$ gentamicin. Following drug addition, the plates are incubated for an additional 48 h at 37 °C, 5% CO₂, 95% air, and 100% relative humidity. For adherent cells, the assay is terminated by the addition of cold TCA. Cells are fixed *in situ* by the gentle addition of 50 μL of cold 50% (w/v) TCA (final concentration, 10% TCA) and incubated for 60 min at 4 °C. The supernatant is discarded, and the plates are washed five times with tap water and air dried. Sulforhodamine B (SRB) solution (100 μL) at 0.4% (w/v) in 1% acetic acid is added to each well, and plates are incubated for 10 min at room temperature. After staining, unbound dye is removed by washing five times with 1% acetic acid and the plates are air dried. Bound stain is subsequently solubilized with 10 mM trizma base, and the absorbance is read on an automated plate reader at a wavelength of 515 nm. For suspension cells, the methodology is the same except that the assay is terminated by fixing settled cells at the bottom of the wells by gently adding 50 μL of 80% TCA (final concentration, 16% TCA). Using the three absorbance measurements [time zero, (Tz), control growth, (C), and test growth in the presence of drug at 10 μM concentration level (Ti)], the percentage growth is calculated at each of the drug concentrations levels. Percentage growth inhibition is calculated as:

$$\left[\frac{(Ti - Tz)}{(C - Tz)} \right] \times 100 \text{ for concentrations for which } Ti > Tz$$

$$\left[\frac{(Ti - Tz)}{Tz} \right] \times 100 \text{ for concentrations for which } Ti < Tz$$

Three dose response parameters are calculated for each experimental agent. Growth inhibition of 50% (GI₅₀) is calculated from $\left[\frac{(Ti - Tz)}{(C - Tz)} \right] \times 100 = 50$, which is the drug concentration resulting in a 50% reduction in the net protein increase (as measured by SRB staining) in control cells during the drug incubation. The drug concentration resulting in total growth inhibition (TGI) is calculated from $Ti = Tz$. The LC₅₀ (concentration of drug resulting in a 50% reduction in the measured protein at the end of the drug treatment as compared to that at the beginning) indicating a net loss of cells following treatment is calculated from $\left[\frac{(Ti - Tz)}{Tz} \right] \times 100 = -50$. Values are calculated for each of these three parameters if the level of activity is reached; however, if the effect is not reached or is exceeded, the value for that parameter is expressed as greater or less than the maximum or minimum concentration tested [30].

4.3.2. MTT assays

Cytotoxicity was determined by MTT for cell viability. The MTT assay was performed according to the method of Skehan and colleagues [26]. Cells were seeded in 96-well flat-bottomed microtiter plates (30,000 cells/well). Cells were incubated overnight with various drugs, and applied as serial dilutions (100 $\mu\text{L}/\text{well}$) at various concentrations. Twenty microliters of MTT (5 mg/ml) were added to each well and incubated for 3 h at 37 °C. The medium was removed and 100 μL of DMSO was added into each well. The plate was gently rotated on an orbital shaker for 10 min to completely dissolve the precipitation. The absorbance was detected at 540 nm with a Microplate Reader (Wallac Victor2, 1420 Multilabel Counter). All measurements were performed in triplicate and each experiment was repeated at least three times. The IC₅₀ value was calculated from the 50% formazan formation compared with a control without addition of drugs. *Data analysis:* the viability was calculated with regard to the untreated cell control [y0], which was set to 100% viability. The resulting curves were fitted by software (Sigma Plot 11.0) to a Hill equation with four parameters.

4.3.3. Apoptosis induction

Determination of apoptosis-associated mitochondrial depolarization loss by flow cytometry [31]. HeLa cells were seeded in 6-well flat-bottomed plates (175,000 cells/well) and incubated overnight with various drugs at serial concentrations.

After treatment, adherent cells were washed with PBS (phosphate buffer saline) and incubated for 30 min at 37 °C with Krebs Ringer Buffered Saline (130 mM NaCl, 3.6 mM KCl, 10 mM HEPES (4-(2-Hydroxyethyl)piperazine-1-ethanesulfonic acid sodium salt), 2 mM NaHCO₃, 0.5 mM NaH₂PO₄, 0.5 mM MgCl₂, 1.5 mM CaCl₂, 4.5 g/L glucose, pH 7.42) supplemented with 20 μM Verapamil (Sigma) and 200 nM tetramethylrhodamine methyl ester TMRM (Invitrogen).

Cells were then detached and collected in the same buffer supplemented with 1% FCS to neutralize the trypsin. At least 2 × 10⁴ cells per sample were analyzed using a FACSCalibur flow cytometer (Becton Dickinson, Mountain View, CA) and the signal from TMRM was read on FL2. The data obtained were acquired, gated, compensated, and analyzed using Cell-Quest software. Mitochondrial depolarization analysis was measured by gating the cells treated overnight with 0.01 μM staurosporine as positive control. Furthermore the average signal of the negative controls (untreated cells) was subtracted from the probe signals. All the experiments were performed in triplicates and replicated twice.

4.3.4. Cell cycle

Analysis of the effect of **6a**, **6b**–**6d** on the HeLa cell cycle was performed accordingly to literature report [38,39]. The effect of **6a**, **6b**–**6d** on the HeLa cell cycle has been analyzed using flow cytometry. Briefly, HeLa cells (1 × 10⁶ cells) were treated with four concentrations (5–10–25–50 μM) of these compounds for 72 h. Cells were washed with PBS, trypsinized, and resuspended in 0.5 mL of PBS. Then, the cells were fixed in chilled 70% ethanol and kept on ice for more than 2 h. After washing the cells twice in 2 mL ice-cold PBS, cells were centrifuged (200 g for 5 min) and the resultant pellet was resuspended in 1 mL PI staining solution and incubated in the dark for 15 min at 37 °C. Cells from each sample were analyzed using a FACSCalibur supported with CellQuest acquisition and data analysis software (Becton Dickinson, Mountain View, CA).

Acknowledgments

This work was supported by CNR fund, RSTL 624/2008. Thanks are due to the NCI, Bethesda, MD (USA) for performing anti-proliferative screening tests. Special thanks to Giovanni Spinelli, Giovanni Ruggieri and Rosalia Scalici for their kind technical support.

Appendix A. Supplementary data

Supplementary data associated with this article can be found in the online version, at <http://dx.doi.org/10.1016/j.ejmech.2013.03.046>. These data include MOL files and InChIKeys of the most important compounds described in this article.

References

- [1] (a) S. Fulda, L. Galluzzi, G. Kroemer, Targeting mitochondria for cancer therapy, *Nat. Rev. Drug Discovery* 9 (2010) 447–464;
(b) S. Fulda, Evasion of apoptosis as a cellular stress response in cancer, *Int. J. Cell. Biol.* (2010) 370835.
- [2] S. Fulda, K.-M. Debatin, Extrinsic versus intrinsic apoptosis pathways in anticancer chemotherapy, *Oncogene* 25 (2006) 4798–4811.
- [3] D.T. Hung, T.F. Jamison, S.L. Shreiber, Understanding and controlling the cell cycle with natural products, *Chem. Biol.* 3 (1996) 623–639.
- [4] L.H. Hartwell, M.B. Kastan, Cell cycle control and cancer, *Science* 266 (1994) 1821–1828.

- [5] M. Segurado, J.A. Tercero, The S-phase checkpoint: targeting the replication fork, *Biol. Cell.* 101 (2009) 617–627.
- [6] K. Vermeulen, Zwi N. Berneman, Dirk R. Van Bockstaele, Cell cycle and apoptosis, *Cell. Proliferation* 36 (2003) 165–175.
- [7] S. Maddica, S. Rao Ande, S. Panigrahi, T. Paranjothy, K. Weglarczyk, A. Zuse, M. Esraghi, K.D. Manda, E. Wiechec, M. Los, Cell survival, cell death and cell cycle pathways are interconnected: implications for cancer therapy, *Drug Resist. Updates* 10 (2007) 13–29.
- [8] A.M. Almerico, A.J. Boulton, An unusual substitution reaction in a benzotriazine derivative, *J. Chem. Soc. Chem. Commun.* (1985) 204–205.
- [9] E.S. Newlands, M.F.G. Stevens, S.R. Wedge, R.T. Wheelhouse, C. Brock, Temozolomide a review of its discovery, chemical properties pre-clinical development and clinical trials, *Cancer Treat. Rep.* 23 (1997) 35–61.
- [10] N.M. Bleehen, E.S. Newlands, S.M. Lee, N. Thatcher, P. Selby, A.H. Calvert, G.J.S. Rustin, M. Brampton, M.F. G Stevens, Cancer research campaign phase II trial of temozolomide in metastatic melanoma, *J. Clin. Oncol.* 13 (1995) 910–913.
- [11] P. Diana, P. Barraja, A. Lauria, A. Montalbano, A.M. Almerico, G. Dattolo, G. Cirrincione, New class of azolo-tetrazinones with potent antitumor activity, *Bioorg. Med. Chem.* 11 (2003) 2371–2380.
- [12] K. Engin, D.B. Leeper, J.R. Cater, A.J. Thistlethwaite, Tupchong, J.D. McFarlane, Extracellular pH distribution in human tumours, *Int. J. Hyperthermia* 11 (1995) 211–216.
- [13] D. Neri, C. Supuran, Interfering with pH regulation in tumours as a therapeutic strategy, *Nat. Drug Discovery* 10 (2011) 767–777.
- [14] A.M. Almerico, F. Mingoia, P. Diana, P. Barraja, A. Lauria, A. Montalbano, G. Cirrincione, G. Dattolo, 1-Methyl-3H-pyrazolo[1,2-a]benzo[1,2,3,4]tetra-3-ones. Design, synthesis, and biological activity of new antitumor agents, *J. Med. Chem.* 48 (2005) 2859–2866.
- [15] A. Lauria, M. Tutone, A.M. Almerico, Virtual lock-and-key approach: the in silico revival of Fischer model by means of molecular descriptors, *Eur. J. Med. Chem.* 46 (2011) 4274–4280.
- [16] A. Lauria, C. Patella, G. Dattolo, A.M. Almerico, Design and synthesis of 4-substituted indolo[3,2-e][1,2,3]triazolo[1,5-a]pyrimidine derivatives with antitumor activity, *J. Med. Chem.* 51 (2008) 2037–2046.
- [17] A. Lauria, M. Ippolito, A.M. Almerico, Inside the Hsp90 inhibitors binding mode through induced fit docking, *J. Mol. Graphics Modell.* 27 (2009) 712–722.
- [18] A. Lauria, M. Ippolito, M. Fazzari, M. Tutone, F. Di Blasi, F. Mingoia, A.M. Almerico, IKK-β inhibitors: an analysis of drug receptor interaction by using molecular docking and pharmacophore 3D QSAR approaches, *J. Mol. Graphics Modell.* 29 (2010) 72–81.
- [19] A. Lauria, M. Ippolito, A.M. Almerico, Combined use of PCA and QSAR/QSPR to predict the drugs mechanism of action. An application to the NCI ACAM Database, *QSAR Comb. Sci.* 28 (2009) 387–395.
- [20] A. Lauria, M. Ippolito, A.M. Almerico, Principal component analysis on molecular descriptors as an alternative point of view in the search of new Hsp90 inhibitors, *J. Comp. Biol. Chem.* 33 (2009) 386–390.
- [21] A. Lauria, C. Patella, I. Abbate, A. Martorana, A.M. Almerico, Lead optimization through VLAK protocol: new annelated pyrrolo-pyrimidine derivatives as antitumor agents, *Eur. J. Med. Chem.* 55 (2012) 375–383.
- [22] A. Lauria, M. Bruno, P. Diana, P. Barraja, A. Montalbano, G. Cirrincione, G. Dattolo, A.M. Almerico, Annelated pyrrolo-pyrimidines from amino-cyanopyrroles and BMMAs as leads for new DNA-interactive ring systems, *Bioorg. Med. Chem.* 13 (2005) 1545–1553.
- [23] A. Lauria, I. Abbate, C. Patella, A. Martorana, G. Dattolo, A.M. Almerico, New Annelated Thieno[2,3-e][1,2,3]triazolo[1,5-a]pyrimidines, with potent anticancer activity, designed through VLAK protocol, *Eur. J. Med. Chem.* 62 (2013) 416–424.
- [24] J.N. Weinstein, K.W. Kohn, M.R. Grever, V.N. Viswanadhan, L.V. Rubinstein, A.P. Monks, D.A. Scudiero, L. Welch, A.D. Koutsoukos, A.J. Chiausa, K.D. Paull, Neural computing in cancer drug development: predicting mechanism of action, *Science* 258 (1992) 447–451.
- [25] W.W. Osdol, T.G. Myers, K.D. Paull, K.W. Kohn, J.N. Weinstein, Use of the Kohonen self-organizing map to study the mechanisms of action of chemotherapeutic agents, *J. Natl. Cancer Inst.* 86 (1994) 1853–1859.
- [26] P. Skehan, R. Storeng, D. Scudiero, A. Monks, J. McMahon, D. Vistica, J.T. Warren, H. Bokesch, S. Kenney, M.R. Boyd, New colorimetric cytotoxicity assay for anticancer-drug screening, *J. Natl. Cancer Inst.* 82 (1990) 1107–1112.
- [27] M.D. Fyaz Ismail, Important fluorinated drugs in experimental and clinical use, *J. Fluorine Chem.* 118 (2002) 27–33.
- [28] M.R. Grever, S.A. Schepartz, B.A. Chabner, The National Cancer Institute: cancer drug discovery and development program, *Semin. Oncol.* 19 (1992) 622–638.
- [29] A. Monks, D. Scudiero, P. Skehan, R. Shoemaker, K. Paull, D. Vistica, C. Hose, J. Langley, P. Cronise, A. Vaigro-Wolff, M. Gray-Goodrich, H. Campbell, M. Boyd, Feasibility of a high-flux anticancer drug screen utilizing a diverse panel of human tumor cell lines in culture, *J. Natl. Cancer Inst.* 83 (1991) 757–766.
- [30] <http://dtp.nci.nih.gov/branches/btb/ivclsp.html>.
- [31] D. Floryk, J. Houstek, Tetramethyl rhodamine methyl ester (TMRM) is suitable for cytofluorometric measurements of mitochondrial membrane potential in cells treated with digitonin, *J. Biosci. Rep.* 19 (1999) 27–34.
- [32] R.J. Youle, A. Strasser, The BCL-2 protein family: opposing activities that mediate cell death, *Nat. Rev. Mol. Cell Biol.* 9 (1) (2008) 47–59.

- [33] G. Palou, R. Palou, A. Guerra-Moreno, A. Duch, A. Travesa, D.G. Quintana, Cyclin regulation by the S phase checkpoint, *J. Biol. Chem.* 285 (2010) 26431–26440.
- [34] LigPrep, Version 2.4, Schrödinger LLC, New York, NY, 2010.
- [35] A.R. Katrinsky, V.S. Lobanov, M. Karelson, Quantum-chemical descriptors in QSAR/QSPR studies, *Chem. Rev.* 96 (1996) 1027–1043.
- [36] C. Venturello, R. D'Alosio, A new synthesis of 2,5-dimethyl-3(2H)furanone, *Synthesis* (1977) 754–755.
- [37] C. Venturello, R. D'Alosio, 2-Aryloxy-2-5-dimethyl-3-oxo-2,3-dihydrofurans. Useful intermediates in the synthesis of 1-aryl-5-methyl-3-pyrazolones, *Synthesis* (1979) 283–287.
- [38] Z. Darzynkiewicz, G. Juan, E. Bedner, Determining cell cycle stages by flow cytometry, in: J.S. Bonifacino, M. Dasso, J.B. Harford, J. Lippincott-Schwartz, K.M. Yamada (Eds.), *Current Protocols in Cell Biology*, John Wiley & Sons, New York, 2001, pp. 8.4.1–8.4.18.
- [39] R. Romagnoli, P.G. Baraldi, C. Lopez Cara, M. Kimatrai Salvador, R. Bortolozzi, G. Basso, G. Viola, J. Balzarini, A. Brancale, Xian-Hua Fu, Jun Li, Su-Zhan Zhang, E. Hamel, One-pot synthesis and biological evaluation of 2-pyrrolidinyl-4-amino-5-(3',4',5'-trimethoxybenzoyl)thiazole: a unique, highly active antimicrotubule agent, *J. Eur. Med. Chem.* 46 (2011) 6015–6024.